Journal of Mathematical Chemistry 10(1992)275–302

MODELLING LIGHT DIATOMICS TRAPPED IN RARE GAS MATRICES: H_2, HD and D_2 in Ar, Kr and Xe

B. SILVI
Dynamiques des Intéractions Moléculaires (URP271), Université Pierre et Marie Curie, 4 Place Jussieu, 75230 Paris Cedex, France

V. CHANDRASEKHARAN
Laboratoire de Photophysique Moléculaire du CNRS, Bâtiment 213, Université Paris Sud, 91405 Orsay, France

M.E. ALIKHANI
Laboratoire de Spectrochimie Moléculaire (URA508), Université Pierre et Marie Curie, 4 Place Jussieu, 75230 Paris Cedex, France

R.D. ETTERS
Physics Department, Colorado State University, Fort Collins, CO 80523, USA

Abstract

The different models allowing the calculations of the rovibrational frequency shifts with respect to the free molecule of a molecular impurity embedded in a rare gas crystal are reviewed. It is shown that models which account for the translational motion of the impurity yield reliable results, the effects of the rare-gas translation seem to be less important. The different models currently used are described in detail and the computational procedures are discussed. Finally, it is shown that for heteronuclear diatomics, the translation–rotation coupling could play an important role.

1. Introduction

Molecules or atoms embedded in rare gas matrices constitute a large body of systems for which extensive spectroscopic studies have been reported. The matrix isolation technique has been developed since the pioneering works of Pimentel [1]. It allows the observation and identification by spectroscopy experiments of unstable species, such as Van der Waals complexes, ion pairs, radicals and reaction intermediates. The applications of this technique have recently been reviewed by Perchard [2].

The interaction between the solute impurity and the host crystal, "the solvent", is generally very weak, and therefore the frequencies of the spectral lines of the matrix isolated systems are very close to their gas phase values. The calculation of the matrix shifts is carried out by a perturbational technique, and the overall quality of the theoretical results is mainly related to the accuracy of the solute–solvent potential for which it constitutes a probe.

For most matrix isolated systems, the mass of the impurity is large and its centre of mass is assumed to be fixed. The translation of the impurity in the cage is, in this case, a classical motion which is not coupled with the rotation and the vibration. In the case of light impurities, this assumption is no longer valid and one has to design specific methods to calculate the frequency shifts which are able to take into account the quantified translation and its coupling with the other motions.

For most molecular impurities, the rotational motion is hindered and is alternatively called libration. For the hydrogen molecule, pure rotational states are observed in the matrix. For the hydrogen rare gas pairs, there exist accurate potentials derived from gas phase experiments on the 1 : 1 complexes by Leroy et al. [3]. These potentials are expressed as a power series of the intramolecular stretching coordinate. Moreover, hydrogen being light has a large centre of mass zero point motion. The hydrogen molecule (H_2, HD, D_2) in rare gas (Ar, Kr, Xe) has been the subject of numerous experimental studies [4–13] as well as theoretical calculations [14–18].

The aim of this contribution is to describe in detail and rationalize the methods used by our group to calculate the frequency shifts of the vibrational and rotational states of a light diatomic impurity trapped in rare gas crystals.

2. Coordinate system and expression of the Hamiltonian

2.1. COORDINATES

The system of interest is made up of a diatomic impurity X, and of a set of N atoms of the rare gas A spherically distributed around the impurity. In principle, this system is described by $6 + 3N$ coordinates. In the case of a host crystal, N tends to infinity. The coordinates used in the following are depicted in fig. 1.

Two frames are necessary. A fixed frame (x, y, z) with its origin at the substitutional site and its axis arbitrarily chosen along the lattice directions is used to define the instantaneous position vectors of the rare gas atoms ($\boldsymbol{r}_i$) and of the impurity centre of mass ($\boldsymbol{r}_0$). The vectors $\boldsymbol{R}_i$ define the classical positions (fixed nuclei) of the rare gas atoms and of the impurity centre of mass, which implies in particular $\boldsymbol{R}_0 = 0$. The diatomic impurity is described by three other coordinates: on the one hand is the internuclear distance r, and on the other hand are the angular coordinates θ, ϕ of the bond with respect to the axis of a local frame (x', y', z'), parallel to the fixed frame but with its origin at the centre of mass of the diatomic.

The dimensionless stretching coordinate ξ defined by:

$$\xi = \frac{r - r_e}{r_e}, \tag{1}$$

in which r_e denotes the equilibrium bond length, will be used instead of r.

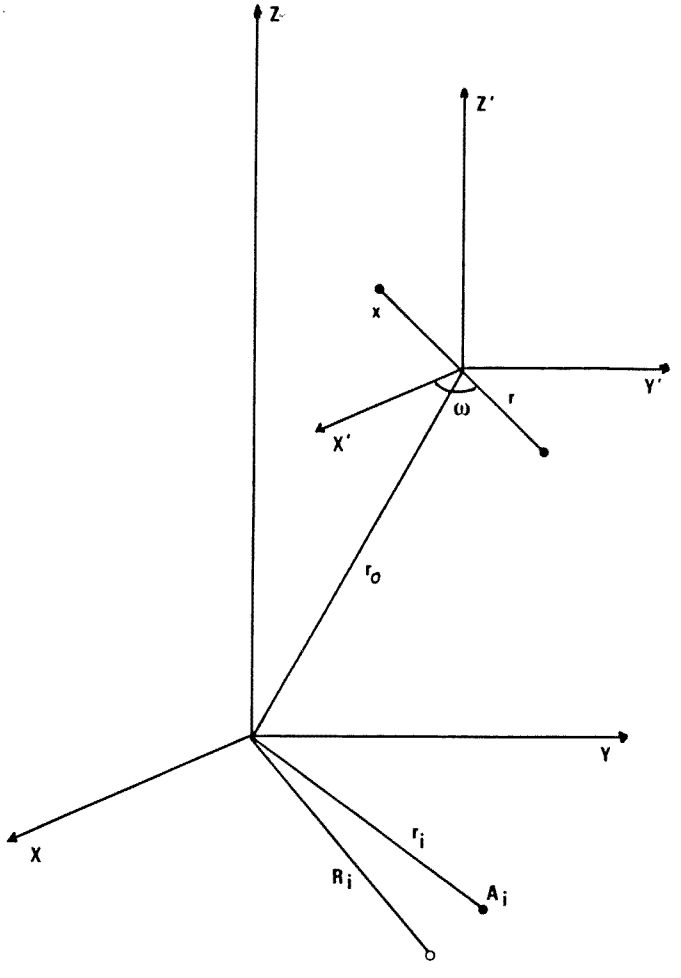

Fig. 1. Coordinate system.

2.2. THE HAMILTONIAN

The Hamiltonian of the whole system can be written as the sum of three contributions:

$$H = H_A + H_X + H_{A-X}, \tag{2}$$

in which

$$H_A = -\frac{\hbar^2}{2M}\sum_{i=1}^{N}\nabla_i^2 + \sum_{i=1}^{N}\sum_{j<i}^{N} V_A(\boldsymbol{r}_i, \boldsymbol{r}_j), \tag{3}$$

$$H_X = -\frac{\hbar^2}{2m}\nabla_0^2 - \frac{\hbar^2}{2\mu}\nabla_\xi^2 + B(\xi)\hat{J}^2 + V_{intra}(\xi), \tag{4}$$

and

$$H_{A-X} = \sum_{i=1}^{N} V_{A-X}(r_0, r_i, \xi, \theta, \phi). \tag{5}$$

M and m are the masses of the matrix atoms and of the molecular impurity, respectively; μ is the reduced mass of the latter. H_A is the Hamiltonian of the rare gas atoms without any interaction potential with the impurity X, H_X is the Hamiltonian of the free molecule which involves three contributions corresponding, respectively, to the translation $((-\hbar^2/2m)\nabla_0^2)$, the rotation $(B(\xi)\hat{J}^2)$, and the vibration $((-\hbar^2/2\mu)\nabla_\xi^2 + V_{intra}(\xi))$, and finally H_{A-X} is the interaction potential which couples the impurity and the host crystal.

2.3. STRUCTURE OF THE POTENTIALS

The rare gas–rare gas potentials are isotropic and are expressed as functions of the only distance $R_{ij} = |\boldsymbol{r}_j - \boldsymbol{r}_i|$. The rare gas–impurity potentials are not isotropic and moreover depend upon the interatomic distance r. In the case of pair potentials, only one angular coordinate ω is necessary to describe the interaction.

In order to account for the ω dependence, V_{A-X} is developed in a series of Legendre polynomials $P_\lambda(\cos\omega)$:

$$V(R_{0i}, r, \omega_i) = \sum_\lambda V_\lambda(R_{0i}, r) P_\lambda(\cos\omega_i). \tag{6}$$

The dependence with respect to r is generally weak and it is possible to use a power series of the stretching coordinate ξ:

$$V(R_{0i}, r, \omega_i) = \sum_\lambda \sum_k \xi^k P_\lambda(\cos\omega_i) V_{\lambda k}(R_{0i}). \tag{7}$$

3. Solution methods

The Schrödinger equation corresponding to the Hamiltonian of eq. (2) cannot be exactly solved; therefore, approximate solutions will be derived from different models.

Three different models will be successively presented: first the correlated particle and then simpler models such as the independent particle or Hartree model, the Einstein model, the Vitko and Coll method [14], and the classical model in which additional approximations are introduced. The following subsections mainly deal with the formalism, the technical points being treated in a next section.

3.1. CORRELATED PARTICLE MODEL

This model was orginally developed by Etters and Danilowicz [19] to treat the hydrogen crystal. The method can be generalized to the embedding problem by

choosing the trial function to be variationally optimized with the following mathematical structure:

$$\Psi(r_0,\ldots,r_N;\xi,\theta,\phi) \approx \exp\left(-\sum_{i<j} u(|r_i - r_j|)\right)\prod_{i=0}^{N}\Phi_i(r_i - R_i)$$

$$\times \chi(\xi)\sum_{JM} C_{JM} Y_J^M(\theta,\phi). \tag{8}$$

The $\Phi(r_i - R_i)$ functions describe the translation of each particle and must satisfy the corresponding limit conditions; the $u(r_{ij})$ functions appearing in the Jastrow prefactor $\exp(-\sum_{i<j} u(r_{ij}))$ have an analytical form such as:

$$u(r_{ij}) \geq 0; \quad u(r_{ij}) \to \infty, \ r \to 0; \quad u(r_{ij}) = 0, \ r \to \infty. \tag{9}$$

These correlation functions cancel the wave function when two particles are in the same place. In the case of electronic wave functions, similar situations are known as Coulomb holes and Fermi holes. Finally, the $\chi(\xi)$ function corresponds to the internal vibrational mode of the impurity, whereas the rotation is expanded on the basis of the spherical harmonics.

The implementation of this method is very intricate and in actual calculations, additional approximations should be introduced.

3.2. INDEPENDENT PARTICLE MODEL

If the Φ_i functions of eq. (8) are localized in the neighbourhood of R_i, the product of the Φ_i and Φ_j functions is close to zero when the ith and jth particles coincide. Therefore, the correlation can be neglected and one can set the Jastrow prefactor equal to 1. Within this approximation, eq. (8) becomes identical to eq. (9) of ref. [16], that is:

$$\Psi \approx \Phi \approx \prod_{i=0}^{N} |R_i\rangle \times |\theta\rangle|\xi\rangle. \tag{10}$$

This structure of the trial wave function allows us to treat the problem by the self-consistent field method. The expectation value of the total Hamiltonian must be minimized with respect to the $|R_i\rangle$, $|\theta\rangle$ and $|\xi\rangle$ functions:

$$\delta\left\{\frac{\langle\Phi|H|\Phi\rangle}{\langle\Phi|\Phi\rangle}\right\} = 0, \tag{11}$$

substituting H by its expression (eqs. (2)–(5)), one obtains, $|\Phi\rangle$ being normalized:

$$E = -\frac{\hbar^2}{2M}\sum_{i=1}^{N}\langle R_i|\nabla_i^2|R_i\rangle + \sum_{i=1}^{N}\sum_{j>i}\langle R_i, R_j|V_A|R_i, R_j\rangle$$
$$-\frac{\hbar^2}{2m}\langle R_0|\nabla_0^2|R_0\rangle - \frac{\hbar^2}{2\mu}\langle\xi|\nabla_\xi^2|\xi\rangle + \langle\xi|V_{intra}|\xi\rangle$$
$$+\langle\xi|B|\xi\rangle\langle\theta|\hat{J}^2|\theta\rangle + \sum_{i=1}^{N}\langle R_i R_0\xi\theta|V_{A-X}|R_i R_0\xi\theta\rangle; \tag{12}$$

variation of $|R_0\rangle$, $|R_i\rangle$, $|\xi\rangle$, and $|\theta\rangle$ yields:

$$\delta\langle\Phi|H|\Phi\rangle = -\frac{\hbar^2}{2m}\Big[\langle\delta R_0|\nabla_0^2|R_0\rangle + \langle R_0|\nabla_0^2|\delta R_0\rangle\Big]$$
$$+\sum_{i=1}^{N}\Big[\langle R_i, \delta R_0, \xi, \theta|V_{A-X}|R_i, R_0, \xi, \theta\rangle + \langle R_i, R_0, \xi, \theta|V_{A-X}|R_i, \delta R_0, \xi, \theta\rangle\Big]$$
$$-\frac{\hbar^2}{2M}\sum_{i=1}^{N}\Big[\langle\delta R_i|\nabla_i^2|R_i\rangle + \langle R_i|\nabla_i^2|\delta R_i\rangle\Big]$$
$$+\sum_{i=1}^{N}\sum_{j>i}\Big[\langle\delta R_i, R_j|V_A|R_i, R_j\rangle + \langle R_i, R_j|V_A|\delta R_i, R_j\rangle\Big]$$
$$+\sum_{i=1}^{N}\Big[\langle\delta R_i, R_0, \xi, \theta|V_{A-X}|R_i, R_0, \xi, \theta\rangle + \langle R_i, R_0, \xi, \theta|V_{A-X}|\delta R_i, R_0, \xi, \theta\rangle\Big]$$
$$-\frac{\hbar^2}{2\mu}\Big[\langle\delta\xi|\nabla_\xi^2 + V_{intra}|\xi\rangle + \langle\xi|\nabla_\xi^2 + V_{intra}|\delta\xi\rangle\Big]$$
$$+\Big[\langle\delta\xi|B|\xi\rangle + \langle\xi\, w B|\delta\xi\rangle\Big]\langle\theta|\hat{J}^2|\theta\rangle$$
$$+\sum_{i=1}^{N}\Big[\langle R_i, R_0, \delta\xi, \theta|V_{A-X}|R_i, R_0, \xi, \theta\rangle + \langle R_i, R_0, \xi, \theta|V_{A-X}|R_i, R_0, \delta\xi, \theta\rangle\Big]$$
$$+\sum_{i=1}^{N}\Big[\langle R_i, R_0, \xi, \delta\theta|V_{A-X}|R_i, R_0, \xi, \theta\rangle + \langle R_i, R_0, \xi, \theta|V_{A-X}|R_i, R_0, \xi, \delta\theta\rangle\Big]$$
$$+\langle\xi|B|\xi\rangle\Big[\langle\delta\theta|\hat{J}^2|\theta\rangle + \langle\theta|\hat{J}^2|\delta\theta\rangle\Big]. \tag{13}$$

This expression can be rewritten as

$$\delta\langle\Phi|H|\Phi\rangle = \langle\delta R_0|F_0|R_0\rangle + \langle R_0|F_0|\delta R_0\rangle + \sum_{i=1}^{N}\left[\langle\delta R_i|F_i|R_i\rangle + \langle R_i|F_i|\delta R_i\rangle\right]$$

$$+ \langle\delta\xi|F_\xi|\xi\rangle + \langle\xi|F_\xi|\delta\xi\rangle + \langle\delta\theta|F_\theta|\theta\rangle + \langle\theta|F_\theta|\delta\theta\rangle, \tag{14}$$

in which the expressions of the F_0, F_i, F_ξ and F_θ operators are, respectively:

$$F_0 = -\frac{\hbar^2}{2m}\nabla_0^2 + \sum_{i=1}^{N}\int R_i^*\xi^*\theta^* V_{A-X} R_i\xi\theta\,\mathrm{d}r_i\,\mathrm{d}\xi\,\mathrm{d}\theta, \tag{15}$$

$$F_i = -\frac{\hbar^2}{2M}\nabla_i^2 + \sum_{j=1}^{N}\int R_j^* V_A R_j \mathrm{d}r_j + \int R_0^*\xi^*\theta^* V_{A-X} R_0\xi\theta\,\mathrm{d}r_i\,\mathrm{d}\xi\,\mathrm{d}\theta, \tag{16}$$

$$F_\xi = -\frac{\hbar^2}{2\mu} + V_{intra} + \langle\theta|\hat{J}^2|\theta\rangle + \sum_{i=1}^{N}\int R_0^* R_i^*\theta^* V_{A-X} R_0 R_i\theta\,\mathrm{d}r_0\,\mathrm{d}r_i\,\mathrm{d}\theta, \tag{17}$$

$$F_\theta = \langle\xi|B|\xi\rangle + \sum_{i=1}^{N}\int R_0^* R_i^*\xi^* V_{A-X} R_0 R_i\xi\,\mathrm{d}r_0\,\mathrm{d}r_i\,\mathrm{d}\xi. \tag{18}$$

The functions $|R_0\rangle$, $|R_i\rangle$, $|\xi\rangle$ and $|\theta\rangle$ are normalized and can be evaluated with the coupled differential equations:

$$F_k|\phi_k\rangle = \varepsilon_k|\phi_k\rangle. \tag{19}$$

The calculation of the functions $|\phi_k\rangle$ must be simultaneously carried out, which implies a self-consistent field resolution technique.

3.3. POSSIBLE APPROXIMATIONS

Within the framework described above, the quantified translation of each molecule or atom of the doped crystal is taken into account. A first approximation is to consider the rare gas atoms as fixed mass points. This approximation has been proposed [15] and is referred to as the Einstein model. It is justified by the very low solute–solvent mass ratio, which is at most 0.1 (D_2 in argon). This model works very nicely and yields frequency shifts very close to those calculated with the independent particle (or Hartree) model.

One can finally neglect the translations completely, and this is the classial model. Because the potential is not averaged, the frequency shifts are overestimated by at most 68%. However, this model is very efficient and the corresponding codes can be run very quickly. Therefore, it can be used in preliminary steps to check physical hypotheses.

In both Hartree and Einstein models, the variational parameters are simultaneously optimized. This is achieved by an iterative process. In the Vilko and Coll approach [14], the impurity translational wave function is calculated in a first step in which the host crystal atoms are assumed to be fixed and unrelaxed. Then the expectation values of the vibrational contributions to the solute–solvent potential are evaluated with respect to translation, allowing the calculation of the matrix shifts.

Although the Vitko and Coll method [14] is, in principle, different to the Einstein model, it implies very similar calculations since the only variational degree of freedom is the translation wave function. The noticeable difference between the numerical results obtained by the Einstein model [15] and those published by Vitko and Coll [14] are to be traced to the different potentials used in these calculations.

4. Calculational procedures

This section describes the numerical procedures used in the actual calculations based on the correlated particle and independent particle models.

4.1. CORRELATED PARTICLE MODEL

The correlation between the impurity and the host crystal is restricted to the first shell of neighbours. The expression of the trial wave function is therefore:

$$\Psi(r_0,\ldots,r_N;\xi,\theta,\phi) = \exp\left(-\sum_{j=1}^{12} u(r_{0j})\right)\prod_{i=0}^{N}\Phi_i(|r_i - R_i|)\chi(\xi)Y_J^M(\theta,\phi), \tag{20}$$

in which:

$$u(r_{ij}) = \tfrac{1}{2}(\kappa/r_{ij})^5 \tag{21}$$

and

$$\Phi_i(r_i) = \left(\frac{\alpha_i}{\pi}\right)^{3/4}\exp\left(-\frac{\alpha_i}{2}r_i^2\right). \tag{22}$$

The variational parameters are on the one hand the exponent of the Gaussian function accounting for the translations of the impurity and on the other hand the κ parameter of the Jastrow prefactor. The relaxation of the first shells surrounding the impurity as well as the exponents of the translational functions of the rare gas atoms are transferred from a preliminary Hartree calculation.

The optimization of the variational parameters is achieved within the simulated annealing framework [21]. Only the parameter-dependent contributions of the Hamiltonian expectation value are required. They correspond to a reduced operator written as:

$$H' = -\frac{\hbar^2}{2M}\nabla_0^2 + \sum_{i=1}^{N} v_{H_2-GR}(r_0, r_i). \tag{23}$$

If the O_h symmetry is assumed, the contributions due to the $P_2(\cos\omega)$ terms vanish after integration over the angular coordinates, so only the $P_0(\cos\omega)$ contributions to the potential remain. Moreover, the potential contributions corresponding to nonzero ξ exponents are neglected. Within these approximations, one obtains:

$$\langle H'\rangle = \frac{3\hbar^2\alpha_0}{4M} + \langle\Psi|\Psi\rangle^{-1}\sum_{j=1}^{12}\int \Phi_0^2(r_0)\Phi_j^2(r_j)\exp(-2u(r_{0j}))v(r_{0j})G(r_0,R_s)\mathrm{d}r_0\mathrm{d}r_j. \tag{24}$$

In this equation:

$$v(r_{0j}) = V_{H_2\text{-}GR}(r_0,r_j) + \frac{\hbar^2}{4M}\nabla_{r_{ij}}^2 u(r_{0j}) \tag{25}$$

is the sum of a potential and a kinetic contribution. Finally,

$$G(r_0,R_s) = \prod_{s\neq j}\int \exp(-2u(r_{0s}))\Phi_s^2(r_s)\mathrm{d}r_s. \tag{26}$$

The analytical expression of the integrals to be evaluated is, in the case of Gaussian basis functions:

$$G(r_0,R_s) = \prod_{s\neq j}\int \exp(-2u(r_{0s}))\mathrm{d}r_s, \tag{27}$$

$$\langle\Psi|\Psi\rangle = \frac{\alpha_0^{3/2}\alpha_1^6}{\pi^{15/2}}\int_0^{2\pi}\mathrm{d}\phi\int_0^{\pi}\sin\theta\,\mathrm{d}\theta\int_0^{\infty} r_0^2\exp(-\alpha_0 r_0^2)\mathrm{d}r_0$$

$$\times\prod_{i=1}^{12}\frac{1}{p_i}\int_{-\infty}^{\infty}|r_i+p_i|\exp(-\kappa^5/|r_i+p_i|^5)\exp(-\alpha_1 r_i^2)\mathrm{d}r_i, \tag{28}$$

with

$$p_i = |R_i - r_0| \tag{29}$$

and

$$\langle\Psi|v|\Psi\rangle = \frac{\alpha_0^{3/2}\alpha_1^6}{\pi^{15/2}}\int_0^{2\pi}\mathrm{d}\phi\int_0^{\pi}\sin\theta\,\mathrm{d}\theta\int_0^{\infty} r_0^2\exp(-\alpha_0 r_0^2)\mathrm{d}r_0$$

$$\times\frac{1}{p_1}\int_{-\infty}^{\infty}|r_1+p_1|\exp(-\kappa^5/|r_1+p_1|^5)v(|r_1+p_1|)\exp(-\alpha_1 r_1^2)\mathrm{d}r_1$$

$$\times\prod_{i=2}^{12}\frac{1}{p_i}\int_{-\infty}^{\infty}|r_i+p_i|\exp(-\kappa^5/|r_i+p_i|^5)\exp(-\alpha_1 r_i^2)\mathrm{d}r_i. \tag{30}$$

The most internal integrals (over r_1, r_i) are numerically evaluated by a Hermite quadrature. The external threefold integral is calculated by a 199 Korobov grid [20]. This technique allows the evaluation of manyfold definite integrals of the form:

$$I = \int_0^1 \ldots \int_1^0 f(x_1, x_2, \ldots, x_s) \mathrm{d}x_1 \mathrm{d}x_2 \ldots \mathrm{d}x_s , \tag{31}$$

with a p-point grid calculated from the s parameters a_s:

$$I = \frac{1}{p} \sum_{k=1}^{p} f\left(\left\{ \frac{a_1 k}{p} \right\}, \left\{ \frac{a_2 k}{p} \right\}, \ldots, \left\{ \frac{a_s k}{p} \right\} \right) - R, \tag{32}$$

where $\{a_i k/p\}$ denotes the fractional part of $a_i k/p$.

The integrals appearing in eqs. (24) and (25) can be easily transformed into integrals bounded in the range (0, 1). The integral over r_0 is calculated in two steps: first over the $(0, r_m)$ interval, secondly over (r_m, ∞) with the auxiliary variable $x = r_m/r$ in order to have finite bounds.

The accuracy of these numerical integrations strongly depends upon the choice of the r_m bound for which preliminary tests have to be performed. A good choice of r_m yields a relative accuracy of the order of $1/p$ for fourfold integrals analytically integrable.

4.2. INDEPENDENT PARTICLE MODEL

The independent particle model used in refs. [13–16] has been improved in order to reduce the uncertainties due to a poor representation of the translational wave functions.

Calculations performed earlier used a single Gaussian function to represent the impurity translation. The exponent of the Gaussian was optimized on the ground-state energy and used afterward to calculate the harmonic translation frequency. This led to a rather simple algorithm and was justified for harmonic or nearly harmonic potentials. With a real potential, such an approximation could introduce uncertainties. The accuracy of the model can be improved by a formalism in which the impurty translation wave function is expressed as a linear combination of Gaussian basis functions:

$$|\phi_1(r_0)\rangle = \sum_j C_{j1} |\chi_j\rangle, \tag{33}$$

with

$$|\chi_j\rangle = \left(\frac{\alpha_j}{\pi} \right)^{3/4} \exp\left(\frac{-\alpha_j}{2} |r_0 - R_0|^2 \right). \tag{34}$$

Since the basis functions are eigenfunctions of the harmonic oscillator, convergence is rapidly achieved when the basis function exponents are simultaneously optimized. The set of basis functions is not an orthonormalized basis set, the expansion coefficients C_{j1} appearing in eq. (28) are calculated by a method analogous to that used in electronic calculations.

4.2.1. Principle

If the $|\phi_i\rangle$ are orthonormalized, one has to minimize the functional

$$\delta\langle\phi_i|H|\phi_i\rangle \tag{35}$$

with the orthonormalization constraint

$$\delta\langle\phi_i|\phi_j\rangle = 0, \tag{36}$$

i.e., to solve the equation:

$$H|\phi_i\rangle = \sum_j \lambda_{i1}|\phi_j\rangle = \varepsilon_i|\phi_i\rangle, \tag{37}$$

in which the λ_{ij} are Lagrange multipliers. The eigenfunctions of H being orthonormalized, one obtains after multiplying on the left by the $\langle\phi_i|$ bra:

$$\lambda_{ii} = \langle\phi_i|H|\phi_i\rangle = \varepsilon_i,$$
$$\lambda_{ij} = 0; \qquad j \neq i. \tag{38}$$

Expressing $\langle\phi_i|$ as a function of $\langle\chi_j|$, one obtains:

$$\sum_k H|\chi_k\rangle C_{ki} = \varepsilon_i \sum_k C_{ki}|\chi_k\rangle. \tag{39}$$

That is, in matricial notation:

$$\mathbf{H}\boldsymbol{\chi}\mathbf{C} = \boldsymbol{\chi}\mathbf{C}\boldsymbol{\varepsilon}. \tag{40}$$

Multiplying to the left by $\boldsymbol{\chi}^{\mathrm{T}}$

$$\boldsymbol{\chi}^{\mathrm{T}}\mathbf{H}\boldsymbol{\chi}\mathbf{C} = \boldsymbol{\chi}^{\mathrm{T}}\boldsymbol{\chi}\mathbf{C}\boldsymbol{\varepsilon}. \tag{41}$$

Now we define the matrices **H** and **S**:

$$\mathbf{H}_{ij} = \langle\chi_i|H|\chi_j\rangle, \tag{42}$$

$$\mathbf{S}_{ij} = \langle\chi_i|\chi_j\rangle; \tag{43}$$

then

$$\mathbf{HC} = \mathbf{SC}\boldsymbol{\varepsilon}, \tag{44}$$

which can be transformed into a standard eigenvalue problem by the following usual technique:

Let $\mathbf{D}$ be an auxiliary matrix such as:

$$\mathbf{C} = \mathbf{S}^{-1/2}\mathbf{D}, \tag{45}$$

$$\mathbf{HS}^{-1/2}\mathbf{D} = \mathbf{S}^{1/2}\mathbf{D}\boldsymbol{\varepsilon}. \tag{46}$$

$\mathbf{S}^{-1/2}$ is symmetric; multiplying again on the right by $\mathbf{S}^{-1/2}$ yields:

$$\mathbf{S}^{-1/2}\mathbf{HS}^{-1/2}\mathbf{D} = \mathbf{D}\boldsymbol{\varepsilon}. \tag{47}$$

It is then possible to simultaneously calculate $\mathbf{D}$ (that is, $\mathbf{C}$) and $\boldsymbol{\varepsilon}$ by diagonalizing the matrix $\mathbf{S}^{-1/2}\mathbf{HS}^{-1/2}$. Finally, the expression of the ground-state energy is:

$$E_0 = \sum_i \sum_j C_{i0} C_{j0} H_{ij}. \tag{48}$$

4.2.2. Calculation of the first excited state

The cage being assumed to be of the O_h symmetry, the ground state belongs to the totally symmetric A_1 representation of the group, whereas the first excited state $|\phi_1\rangle$, which is triply degenerate, belongs to the F_{1u} representation. It is the lowest state of this representation and therefore the variational principle holds. The basis functions used to carry out the calculations are the $\upsilon = 1$ three-dimensional harmonic oscillator eigenfunctions:

$$|\chi(\alpha)\rangle = N_\alpha r \exp^{-\alpha r^2/2} Y_1^0(\Omega). \tag{49}$$

The calculation of the expansion coefficients of $|\phi_1\rangle$ over the basis function is carried out by the method previously outlined.

4.3. OPTIMIZATION OF THE VARIATIONAL PARAMETERS

The approximate ground-state energy resulting from eq. (24) might have multiple minima depending on the parameters chosen. For these reasons, standard gradient procedures could fail. The simulated annealing method [21] is suitable for such optimizations and is sketched below.

Let $F(x_1, \ldots, x_i, \ldots, x_n)$ be an N variable function; the set of the values of the variables $\{x_i\}$ is called a configuration. Starting from an initial configuration $\{x_i\}$, the following configurations are generated by increasing successively each variable by an amount of Δx_k proportional to a random number lying in the range $[-0.5, 0.5]$. If

$$\Delta F = F(x_1, \ldots, x_k + \Delta x_k, \ldots) - F)x_1, \ldots, x_k, \ldots) < 0, \tag{50}$$

then the new configuration is accepted; if ΔF is positive, a random number b in the range [0, 1] is generated. If $\exp(-\Delta F/kT) > b$ (T represents a virtual temperature and k is the Boltzmann constant), the new configuration is accepted. This process is performed until a good convergence on the $\{x_k\}$ is obtained and the procedure reiterated with lower virtual temperatures.

4.4. CALCULATION OF THE FREQUENCY SHIFTS

Once the variational parameters are optimized, the frequency shifts are calculated as follows: in a first step, the expectation values of the V_{0k} operators defined by eq. (7) are evaluated. In a second step, these expectation values are added to the intramolecular potential:

$$V_{0k}^{\text{eff}}(\xi) = V_{intra}(\xi) + \sum_{k=1}^{3} \xi^k \langle V_{0k} \rangle. \tag{51}$$

The minimum of this effective potential together with the coefficients of its expansion in power series of ξ are calculated. The rovibrational frequencies of the impurity are computed by the WKB method with the effective potential.

In our calculation, the free molecular intramolecule potential is taken from Hamaguchi et al. [22]. For the isolated H_2, HD and D_2 species, the WKB frequencies are very close to the experimental ones, as shown in table 1.

Table 1

Calculated and observed ( ) frequencies.

	H_2		HD		D_2	
$S_0(0)$	354.38	(354.38)	267.04	(267.09)	179.01	(179.06)
$S_0(1)$	587.06	(587.05)			297.44	(297.52)
$Q_2(0)$	4161.17	(4161.17)	3631.90	(3632.10)	2993.00	(2993.55)
$Q_1(1)$	4155.27	(2155.24)			2990.89	(2991.45)

5. Potentials

Two kinds of pair potentials have to be considered; on the one hand is the rare gas–rare gas potential describing the host crystal, and on the other hand is the rare gas–impurity potential which accounts for the description of the defect.

5.1. RARE GAS POTENTIALS

The rare gas–rare gas potentials used in the calculations are those of Aziz and Chen [23], Aziz [24], and Barker et al. [25] for the Ar–Ar, Kr–Kr and

Xe–Xe pairs, respectively. In order to simulate three-body forces, a C_9 coefficient has been added to the original potentials. The analytical form of the Ar–Ar and Kr–Kr potentials is:

$$V(x)=\varepsilon\left[Ax^{\gamma}\exp(-\alpha x)-\left(\frac{C_6}{x^6}+\frac{C_8}{x^8}+\frac{C_9}{x^9}+\frac{C_{10}}{c^{10}}\right)F(x)\right], \tag{52}$$

with

$$x=\frac{r}{r_0};\quad F(x)=\exp\left(-\left(\frac{D}{x}-1\right)^2\right),\quad x<D;\quad F(x)=1,\quad x\geq D. \tag{53}$$

The analytical form of the Barker et al. [25] potential is:

$$V(x)=\varepsilon\left[\sum_{i=0}^{5}A_i(x-1)^i\exp\alpha(1-x)-\left(\frac{C_6}{x^6+\delta}+\frac{C_8}{x^8+\delta}+\frac{C_9}{x^9+\delta}+\frac{C_{10}}{x^{10}+\delta}\right)+u_1(x)\right], \tag{54}$$

with $x=r/r_0$ and

$$\begin{aligned} u_1(x)&=(P(x-1)^4+Q(x-1)^5)\exp\alpha'(1-x) && x>1,\\ &=0, && x<1. \end{aligned} \tag{55}$$

Table 2 reports the numerical values of the rare gas potential constants.

Table 2

Ar–Ar, Kr–Kr and Xe–Xe potential parameters.

	Argon	Krypton	Xenon
ε [cm^{-1}]	99.234	138.3	195.3
A	0.950272 10^7	0.1215312 10^8	
A_0			0.2402
A_1			−4.8169
A_2			−10.9
A_3			−25.0
A_4			−50.7
A_5			−200.0
γ	0.0	2.4	
α	16.345655	19.595151	12.5
α'			12.5
C_6	1.0914254	1.1561739	1.0544
C_8	0.6002595	0.5414923	0.1660
C_9	−0.0910328	−0.1110328	−0.1398
C_{10}	0.3700113	0.2839735	0.0323
D	1.4	1.28	
δ			0.01
P			59.3
Q			71.1
r_0 [Å]	3.759	4.012	4.3623

Table 3

H_2–rare gas potential parameters.

	Argon	Krypton	Xenon
ε [cm^{-1}]	50.87	58.73	64.78
R_0 [Å]	3.5727	3.7181	3.9366
β	12.897447	12.6378219	13.7151144
A^{00}	4.449289188 10^5	3.683724293 10^5	9.139646204^5
A^{01}	5.483368724 10^5	3.388919921 10^5	9.138093218^5
A^{02}	2.475125632 10^5	1.662118551 10^5	4.241081060^5
A^{03}	0.0	0.0	0.0
A^{20}	0.946442319 10^5	0.830700909 10^5	0.966400266^5
A^{21}	7.665032784 10^5	2.821389524 10^5	1.572278408^5
A^{22}	6.718067649 10^5	1.991134960 10^5	2.322814468^5
A^{23}	0.0	0.0	0.0
C_6^{00}	1.271397189	1.226457182	1.112474593
C_6^{01}	1.094630443	1.078225363	1.026612460
C_6^{02}	0.028840393	0.035865655	0.048572250
C_6^{03}	– 0. 238871427	– 0.237750948	– 0.231454446
C_6^{20}	0.127612358	0.125352560	0.118423377
C_6^{21}	0.279801909	0.278740269	0.270113145
C_6^{22}	0.053928037	0.055580497	0.057490298
C_6^{23}	– 0.098261515	– 0.097807221	– 0.094199471
C_8^{00}	0.842898814	0.969596862	0.898012760
C_8^{01}	0.850248127	0.658479797	0.802902140
C_8^{02}	0.318960195	0.397546525	0.446359029
C_8^{03}	0.0	0.0	0.0
C_8^{20}	0.209166496	0.278808845	0.204631184
C_8^{21}	1.703680729	0.874675296	0.459913546
C_8^{22}	1.494453460	0.596049103	0.256659819
C_8^{23}	0.0	0.0	0.0

The damping function $F(x)$ of eq. (52) as well as the damping factor δ in eq. (54) are introduced in order to keep the potential finite and repulsive when r tends to zero. They prevent against the "black hole" behaviour of 6–exp type potentials during the geometry optimization procedure.

The two rare gas–rare gas potential-dependent constants which are mainly involved in actual simulations of the doped crystal at low pressure are on the one hand the pair potential equilibrium distance and on the other hand the curvature of the potential at the minimum. Close values of these constants can be obtained by

different kinds of pair potential and therefore the results do not depend very much upon the nature of the potential.

5.2. HYDROGEN–RARE GAS POTENTIALS

The potentials proposed by Le Roy and Carley [3] have the Buckingham Corner form:

$$V^{\lambda k}(R) = A^{\lambda k} \exp(-\beta R) - \left[\frac{C_6^{\lambda k}}{R^6} + \frac{C_8^{\lambda k}}{R^8}\right] D(R). \tag{56}$$

$D(R)$ is a damping function which tends to zero with R:

$$\begin{aligned} D(R) &= \exp\left(-4\left(\frac{R_0}{R} - 1\right)^3\right) \quad R \leq R_0, \\ &= 1 \qquad\qquad\qquad\qquad\quad R > R_0. \end{aligned} \tag{57}$$

The potential parameters have been optimized in order to reproduce accurately the rovibrational levels of H_2 rare gas 1:1 complexes. These parameters are given in table 3.

6. Numerical results and discussion

6.1. TRANSLATION FREQUENCIES

The translation frequencies calculated by the independent particle or Hartree model are reported in table 4. These results have been obtained by expressing the translational wave functions with a single basis function. The expansion over three Gaussian functions yields almost identical results; the discrepancies are at most

Table 4

Impurity translation frequencies [cm^{-1}], ( ) corresponding harmonic frequency.

	Ar	Kr	Xe
H_2	135.4 (127)	111.3 (108)	91.2 (98)
HD	107.1 (97)	87.2 (82)	70.4 (75)
D_2	90.9 (84)	74.5 (70)	58.6 (63)

0.1 cm^{-1}, that is, of the order of the numerical noise. In the cases of the argon and krypton matrices, the anharmonic frequencies are found to be larger than the harmonic ones because of a positive fourth-order term in the effective potential. An opposite result is observed for xenon.

Table 5

Calculated and observed frequency shifts [cm^{-1}].

	Classical model	Einstein model	Hartree model	Correlated model	Exp.
			H_2 in argon		
$S_0(0)$	−2.4	−1.9	−1.8	−2.0	−1.5
$S_0(1)$	−3.9	−3.1	−2.9	−3.3	−2.3
$Q_1(0)$	−32.1	−22.6	−21.0	−24.8	−19.0
$Q_1(1)$	−32.1	−22.6	−21.0	−24.8	−19.1
			HD in argon		
$S_0(0)$	−1.7	−1.4	−1.3	−1.5	−1.3
$Q_1(0)$	−25.8	−17.7	−16.1	−22.5	−16.5
			D_2 in argon		
$S_0(0)$	−1.2	−1.0	−1.0	−1.0	−0.9
$S_0(1)$	−2.0	−1.7	−1.6	−1.6	−1.3
$Q_1(0)$	−23.1	−18.4	−17.4	−17.4	−14.5
$Q_1(1)$	−23.1	−18.4	−17.4	−17.4	−14.7
			H_2 in krypton		
$S_0(0)$	−2.6	−2.3	−2.2	−2.4	−2.7
$S_0(1)$	−4.3	−3.7	−3.7	−4.0	−3.0
$Q_1(0)$	−38.0	−31.4	−31.3	−34.5	−28.7
$Q_1(1)$	−38.0	−31.4	−31.3	−34.5	−29.1
			HD in krypton		
$S_0(0)$	−1.9	−1.7	−1.6	−1.8	−2.0
$Q_1(0)$	−31.9	−26.5	−26.1	−29.6	−25.4

. . . continued

Table 5 (continued)

	D_2 in krypton				
	Classical model	Einstein model	Hartree model	Correlated model	Exp.
$S_0(0)$	−1.3	−1.2	−1.2	−1.2	−1.5
$S_0(1)$	−2.1	−2.0	−1.9	−2.0	−2.2
$Q_1(0)$	−27.0	−23.9	−23.7	−24.6	−21.2
$Q_1(1)$	−27.0	−23.9	−23.7	−24.6	−21.4

	H_2 in xenon				
	Classical model	Einstein model	Hartree model	Correlated model	Exp.
$S_0(0)$	−3.0	−2.8	−2.7	−2.9	−2.8
$S_0(1)$	−5.0	−4.6	−4.6	−4.7	−3.8
$Q_1(0)$	−46.3	−42.2	−41.6	−43.3	−37.7
$Q_1(1)$	−46.3	−42.3	−41.6	−43.3	−37.9

	HD in xenon				
	Classical model	Einstein model	Hartree model	Correlated model	Exp.
$S_0(0)$	−2.2	−2.1	−2.1	−2.2	−2.1
$Q_1(0)$	−39.8	−37.0	−35.7	−38.1	−31.9

	D_2 in xenon				
	Classical model	Einstein model	Hartree model	Correlated model	Exp.
$S_0(0)$	−1.4	−1.5	−1.4	−1.4	−1.7
$S_0(1)$	−2.5	−2.3	−2.3	−2.4	−2.7
$Q_1(0)$	−32.7	−30.5	−30.5	−31.2	−26.8
$Q_1(1)$	−32.7	−30.5	−30.5	−31.2	−26.8

The only available experimental results concern on the one hand H_2 and D_2 in an argon matrix [4,5] and on the other hand H_2 in krypton [4]. The experimental values have been deduced from combination bands observed at 82 K. Vitko and Coll [14] have shown that the translational frequency increases when the temperature is lowered. In the case of H_2 in argon, the calculation indicates an increase of 15 cm^{-1} when the temperature decreases from 82 to 12 K. Our calculated frequencies

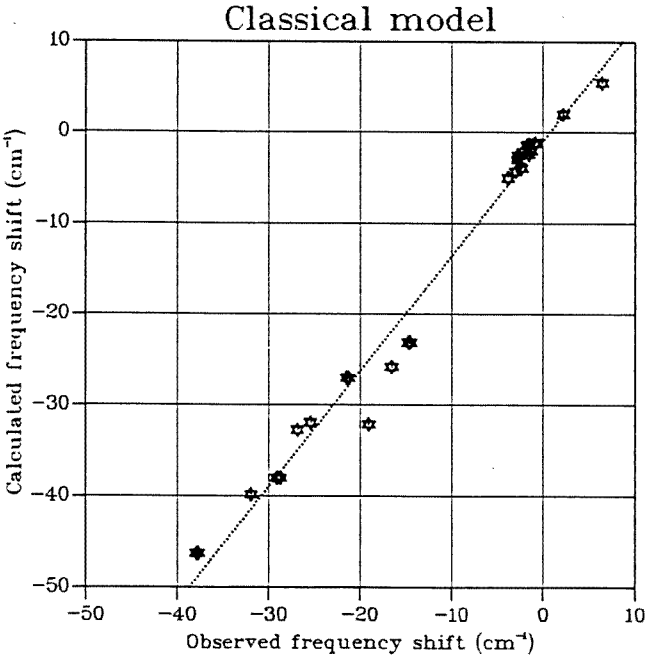

Fig. 2. Classical model. Calculated versus observed frequency shifts.

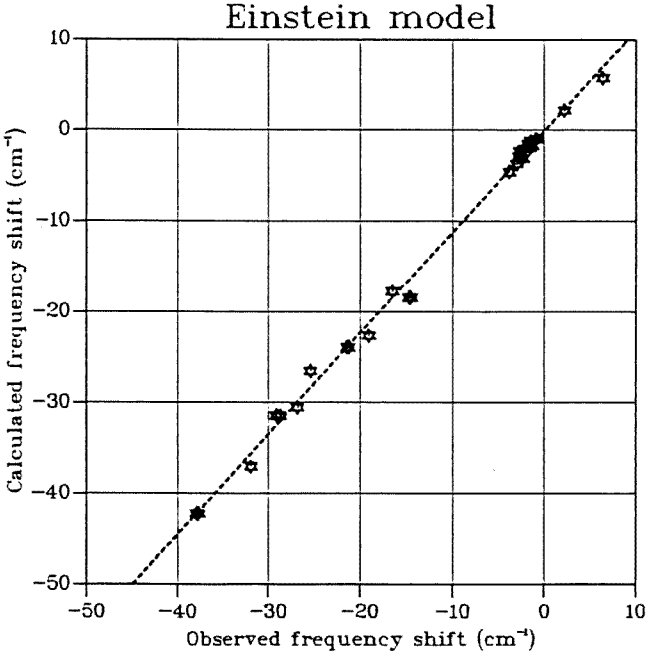

Fig. 3. Einstein model. Calculated versus observed frequency shifts.

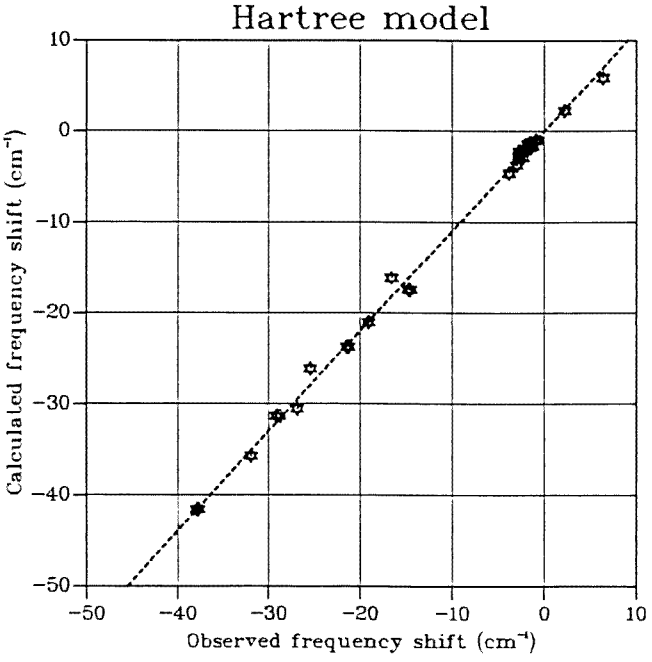

Fig. 4. Hartree model. Calculated versus observed frequency shifts.

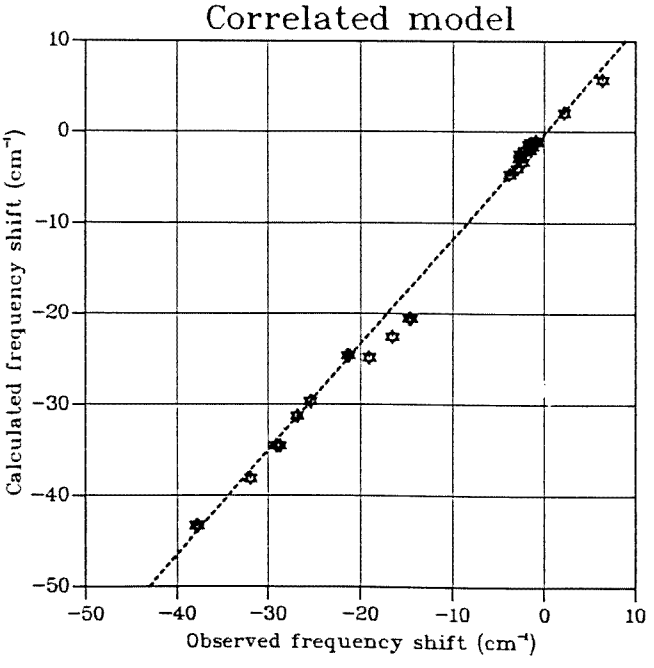

Fig. 5. Correlated model. Calculated versus observed frequency shifts.

nevertheless appear more or less overestimated, at least for argon and krypton matrices, for which the experimental values are, respectively, 112 and 106 cm^{-1} for H_2.

6.2. VIBRATION–ROTATION LINE FREQUENCY SHIFTS

Table 5 compares the frequency shifts of the vibration–rotation lines calculated by the different models to the experimental ones.

The four models qualitatively account for the observed phenomena: the sign and the order of magnitude of the frequency shifts are correctly predicted as well as their evolution with the nature of the host crystal. However, the calculated frequency shifts are always larger than the experimental ones. This overestimation is particularly important in the case of the classical model for which the $\Delta\nu_{calc}/\Delta\nu_{obs}$ ratio is 1.68, 1.32 and 1.24 for argon, krypton and xeonon, respectively, for the $Q_1(0)$ line of the H_2 species. For the D_2 molecule, this ratio is slightly lower (1.61, 1.28 and 1.22). If the impurity translation is accounted for, this ratio is lowered to 1.1 for the three matrices. Figures 2–5 show the calculated frequency shifts as functions of the experimental ones. For the classical model, the points are scattered around the linear regression line and consequently the overall quality of the calculations depends upon the nature of the host cystal. In the case of the three more sophisticated models, the regression coefficient is of the order of 0.99, indicating a homogeneous quality of the calculated results.

From these results, it appears that the "Einstein" model is accurate enough for this kind of problem. More sophisticated physical models fail in significantly improving the agreement between calculated and observed shifts. Although the independent particle model slightly lowers the frequency shifts with respect to the "Einstein" model, the correlated particle model which is expected to be more accurate yields, on the contrary, larger shifts. This should be due to an awkward choice of the Jastrow prefactor or to a variational artefact.

It should be possible to improve the whole set of these results by scaling the hydrogen–rare gas pair potential. This would lead to a lowering of both the impurity translational frequency and of the frequency shifts.

7. Translation–rotation coupling

In the different models described above, the coupling between the translational and rotational motions of the impurity has been neglected. In these models, the frequency shifts of the rotational lines S_0 and S_1 are explained by the lowering of the B_e rotational constant due to the matrix field. For the centrosymmetric species, namely H_2 and D_2, the results of the calculations are in quantitative agreement with experiment. On the contrary, for HD there is a large discrepancy between theory and experiment. Taking into account translation–rotation coupling allows one to overcome this difficulty.

The effect of a crystalline surrounding on the rotational states of a molecule has been theoretically analyzed by several authors [26,27]; in this work, we have considered a method originally proposed by Allavena and Rios [27].

Consider a molecule AB with a mass M and a rotational constant B subject to the crystal field applied on the molecular centre of interaction which, in general, does not coincide with the centre of mass. For a system belonging to point groups which possess inversion among their operators, the interaction and mass centres coincide. In order to simplify the formalism, the simple case of a rigid rotator localized in a rigid cage is treated herein.

In this system, the centre of mass coordinates are X, Y, Z, whereas those of the interaction centre are $X' = X - d\sin\theta\cos\phi$, $Y' = Y - d\sin\theta\cos\phi$, $Z' = Z - d\sin\theta\cos\phi$, respectively. The Hamiltonian of this system is written as:

$$H = -\frac{\hbar^2}{2M}\left[\frac{\partial^2}{\partial X^2} + \frac{\partial^2}{\partial Y^2} + \frac{\partial^2}{\partial Z^2}\right] + B\hat{J}^2 + V(X',Y',Z'). \tag{58}$$

Expanding the potential about the centre of mass yields:

$$V(X',Y',Z') = V(X,Y,Z) - d\sum_{\tau=X,Y,Z}\left(\frac{\partial V}{\partial \tau}\right)\mu_\tau + d^2\sum_{\tau,\tau'}\left(\frac{\partial^2 V}{\partial\tau\partial\tau'}\right)\mu_\tau\mu_{\tau'} + \ldots, \tag{59}$$

with $\mu_X = \sin\theta\cos\phi$, $\mu_Y = \sin\theta\cos\phi$ and $\mu_X = \sin\theta\cos\phi$. Restricting the expansion to the second order in d, the Hamiltonian (eq. (48)) can be rewritten as the sum of the unperturbed Hamiltonian H^0 and of a perturbation H^1:

$$H = H^0 + H^1,$$

$$H^0 = -\frac{\hbar^2}{2M}\left[\frac{\partial^2}{\partial X^2} + \frac{\partial^2}{\partial Y^2} + \frac{\partial^2}{\partial Z^2}\right] + B\hat{J}^2 + V(X,Y,Z),$$

$$H^1 = dH^{\mathrm{I}} + d^2H^{\mathrm{II}} = -d\sum_{\tau=X,Y,Z}\left(\frac{\partial V}{\partial\tau}\right)\mu_\tau + d^2\sum_{\tau,\tau'}\left(\frac{\partial^2 V}{\partial\tau\partial\tau'}\right)\mu_\tau\mu_{\tau'} + \ldots. \tag{60}$$

The H^0 eigenfunctions are:

$$|\Psi^0_{nlm}\rangle = |\Phi^0_n\rangle|Y^m_l\rangle, \tag{61}$$

in which the $|\Phi^0_n\rangle$ are the eigenfunctions of the translation Hamiltonian and are solutions of the equation:

$$\left\{-\frac{\hbar^2}{2M}\left[\frac{\partial^2}{\partial X^2} + \frac{\partial^2}{\partial Y^2} + \frac{\partial^2}{\partial Z^2}\right] + V(X,Y,X)\right\}|\Phi^0_n\rangle = E^0_n|\Phi^0_n\rangle. \tag{62}$$

The perturbation corrections are restricted to the two first orders of the states $|\Psi_{0lm}\rangle$ and only the d and d^2 terms are taken into account. The expressions of these corrections are, respectively:

$$E^{(1)}_{0lm} = \langle \Psi_{0lm}|H^1|\Psi_{0lm}\rangle = d\langle \Psi_{0lm}|H^{\mathrm{I}}|\Psi_{0lm}\rangle + d^2\langle \Psi_{0lm}|H^{\mathrm{II}}|\Psi_{0lm}\rangle, \tag{63}$$

$$E^{(2)}_{0lm} = -d^2 \sum_n \sum_{l'} \sum_{m'} \frac{|\langle \Psi_{0lm}|H^{\mathrm{I}}|\Psi_{0l'm'}\rangle|^2}{E^0_n - E^0_0 + B[l'(l'+1) - l(l+1)]}. \tag{64}$$

The following matrix elements have thus to be evaluated: $\langle \Psi_{0lm}|H^{\mathrm{I}}|\Psi_{nl'm'}\rangle$ and $\langle \Psi_{0lm}|H^{\mathrm{II}}|\Psi_{0lm}\rangle$. The expressions of the matrix elements of H^{I} and H^{II} are:

$$\langle \Psi^0_{0lm}|H^{\mathrm{I}}|\Psi^0_{nl'm'}\rangle = \sum_{\tau=X,Y,Z} \left\langle \Phi^0_0 \left| \frac{\partial V}{\partial \tau} \right| \Phi^0_n \right\rangle \int_\Omega Y_l^{m*} \mu_\tau Y_{l'}^{m'} \mathrm{d}\Omega\,, \tag{65}$$

$$\langle \Psi^0_{0lm}|H^{\mathrm{II}}|\Psi^0_{nlm}\rangle = \sum_\tau \sum_{\tau'} \left\langle \Phi^0_0 \left| \frac{\partial^2 V}{\partial \tau \partial \tau'} \right| \Phi^0_0 \right\rangle \int_\Omega Y_l^{m*} \mu_\tau \mu_{\tau'} Y_l^m \mathrm{d}\Omega\,. \tag{66}$$

In a first step, the direction cosines μ_τ are expressed in terms of spherical harmonics:

$$\mu_X = \sin\theta\cos\phi = -\left(\frac{2\pi}{3}\right)^{1/2}\left[Y_1^1(\Omega) + Y_1^{-1}(\Omega)\right],$$

$$\mu_Y = \sin\theta\cos\phi = \mathrm{i}\left(\frac{2\pi}{3}\right)^{1/2}\left[Y_1^1(\Omega) - Y_1^{-1}(\Omega)\right],$$

$$\mu_Z = \cos\theta = \left(\frac{4\pi}{3}\right)^{1/2} Y_1^0(\Omega), \tag{67}$$

$$\mu_X\mu_X = \left(\frac{2\pi}{15}\right)^{1/2}\left[Y_2^2(\Omega) + Y_2^{-1}(\Omega)\right] - \left(\frac{4\pi}{45}\right)^{1/2} Y_2^0(\Omega) + \left(\frac{4\pi}{9}\right)^{1/2} Y_0^0(\Omega),$$

$$\mu_X\mu_Y = -\mathrm{i}\left(\frac{2\pi}{15}\right)^{1/2}\left[Y_2^2(\Omega) - Y_2^{-2}(\Omega)\right],$$

$$\mu_X\mu_Z = -\left(\frac{4\pi}{15}\right)^{1/2}\left[Y_2^1(\Omega) + Y_2^{-1}(\Omega)\right],$$

$$\mu_Y\mu_Y = -\left(\frac{2\pi}{15}\right)^{1/2}\left[Y_2^2(\Omega) + Y_2^{-2}(\Omega)\right] - \left(\frac{4\pi}{45}\right)^{1/2} Y_2^0(\Omega) + \left(\frac{4\pi}{9}\right)^{1/2} Y_0^0(\Omega),$$

$$\mu_Y\mu_Z = \mathrm{i}\left(\frac{4\pi}{15}\right)^{1/2}\left[Y_2^1(\Omega) - Y_2^{-1}(\Omega)\right],$$

$$\mu_Z\mu_Z = \left(\frac{16\pi}{45}\right)^{1/2} Y_2^0(\Omega) + \left(\frac{4\pi}{9}\right)^{1/2} Y_0^0(\Omega). \tag{68}$$

The integrals over the angular coordinates are then expressed as sums of the $C_{Lll'}^{Mmm'}$ coefficients defined by Harris [28]:

$$C_{Lll'}^{Mmm'} = \int_\Omega Y_L^{M*} Y_l^m Y_{l'}^{m'} \mathrm{d}\Omega. \tag{69}$$

Unless the following requirements are satisfied, these coefficients are zero:

(1) $M = m + m'$;

(2) $L + l + l' = 2k; \quad k \in N$;

(3) $|l - l| \le L \le l + l'$;

(4) $L \ge |M|$. (70)

The nonzero coefficients are functions of the 3_j symbols:

$$C_{Lll'}^{Mmm'} = (-1)^M \left[\frac{(2L+1)(2l+1)(2l'+1)}{4\pi}\right]^{1/2} \begin{pmatrix} L & l & l' \\ 0 & 0 & 0 \end{pmatrix} \begin{pmatrix} L & l & l' \\ M & m & m' \end{pmatrix}. \tag{71}$$

The nonzero matrix elements are therefore:

$$\langle \Psi_{0lm} | H^1 | \Psi_{nl+1m-1} \rangle = \left(\frac{2\pi}{3}\right)^{1/2} C_{ll+11}^{mm-11} \left\langle \Phi_0^0 \left| \frac{\partial V}{\partial X} - \mathrm{i}\frac{\partial V}{\partial Y} \right| \Phi_n^0 \right\rangle,$$

$$\langle \Psi_{0lm} | H^1 | \Psi_{nl+1m+1} \rangle = \left(\frac{2\pi}{3}\right)^{1/2} C_{ll+11}^{mm+1-1} \left\langle \Phi_0^0 \left| \frac{\partial V}{\partial X} + \mathrm{i}\frac{\partial V}{\partial Y} \right| \Phi_n^0 \right\rangle,$$

$$\langle \Psi_{0lm} | H^1 | \Psi_{nl-1m-1} \rangle = \left(\frac{2\pi}{3}\right)^{1/2} C_{ll-11}^{mm-11} \left\langle \Phi_0^0 \left| \frac{\partial V}{\partial X} - \mathrm{i}\frac{\partial V}{\partial Y} \right| \Phi_n^0 \right\rangle,$$

$$\langle \Psi_{0lm}|H^1|\Psi_{nl-1m+1}\rangle = \left(\frac{2\pi}{3}\right)^{1/2} C_{ll-11}^{mm+11}\left\langle \Phi_0^0\left|\frac{\partial V}{\partial X}+\mathrm{i}\frac{\partial V}{\partial Y}\right|\Phi_n^0\right\rangle,$$

$$\langle \Psi_{0lm}|H^1|\Psi_{nl+1m}\rangle = -\left(\frac{4\pi}{3}\right)^{1/2} C_{ll+11}^{mm0}\left\langle \Phi_0^0\left|\frac{\partial V}{\partial Z}\right|\Phi_n^0\right\rangle,$$

$$\langle \Psi_{0lm}|H^1|\Psi_{nl-1m}\rangle = -\left(\frac{4\pi}{3}\right)^{1/2} C_{ll-11}^{mm0}\left\langle \Phi_0^0\left|\frac{\partial V}{\partial Z}\right|\Phi_n^0\right\rangle,$$

$$\langle \Psi_{0lm}|H^1|\Psi_{nlm}\rangle = \left[\frac{1}{3}-\left(\frac{4\pi}{45}\right)^{1/2} C_{ll2}^{mm0}\right]\left\langle \Phi_0^0\left|\frac{\partial^2 V}{\partial X^2}+\frac{\partial^2 V}{\partial Y^2}+\frac{\partial^2 V}{\partial Z^2}\right|\Phi_n^0\right\rangle,$$

$$+3\left(\frac{2\pi}{45}\right)^{1/2} C_{ll2}^{mm0}\left\langle \Phi_0^0\left|\frac{\partial^2 V}{\partial Z^2}\right|\Phi_n^0\right\rangle. \tag{72}$$

The values of the $C_{Ll l'}^{Mmm'}$ coefficients are give by

$$C_{ll2}^{mm0} = -\left(\frac{5}{4\pi}\right)^{1/2}\frac{3m^2-l^2-l}{(2l+3)(2l-1)},$$

$$C_{ll+1}^{mm0} = \left[\frac{3(l-m+1)(l+m+1)}{4\pi(2l+3)(2l+1)}\right]^{1/2},$$

$$C_{ll-11}^{mm0} = \left[\frac{3(l-m)(l+m)}{4\pi(2l+1)(2l-1)}\right]^{1/2},$$

$$C_{ll+11}^{mm-11} = -\left[\frac{3(l-m+1)(l-m+2)}{8\pi(2l+3)(2l+1)}\right]^{1/2},$$

$$C_{ll-11}^{mm-11} = \left[\frac{3(l+m-1)(l+m)}{8\pi(2l+1)(2l-1)}\right]^{1/2},$$

$$C_{ll+11}^{mm+1-1} = \left[\frac{3(l+m+1)(l+m+2)}{8\pi(2l+3)(2l+1)}\right]^{1/2},$$

$$C_{ll-11}^{mm+1-1} = -\left[\frac{3(l-m-1)(l-m)}{2\pi(2l+1)(2l-1)}\right]^{1/2}. \tag{73}$$

Substituting into eq. (54), one obtains:

$$E^{(1)}_{0lm} = d^2\left\{\frac{l^2+l-1+m}{(2l-1)(2l+3)}\left\langle\Phi_0^0\left|\frac{\partial^2 V}{\partial X^2}+\frac{\partial^2 V}{\partial Y^2}\right|\Phi_0^0\right\rangle+\frac{2l^2+2l-2m^2}{(2l-1)(2l+3)}\left\langle\Phi_0^0\left|\frac{\partial^2 V}{\partial Z^2}\right|\Phi_0^0\right\rangle\right\}, \tag{74}$$

$$\begin{aligned}E^{(2)} = -\,d^2\Bigg\{&\frac{(l+1)(l+2)+m^2}{2(2l+1)(2l+3)}\sum_n\frac{|\langle\Phi_0^0|\frac{\partial V}{\partial X}+\frac{\partial V}{\partial Y}|\Phi_n^0\rangle|^2}{E_n-E_0+2Bhc(l+1)}\\&+\frac{(l+1)^2-m^2}{(2l+1)(2l+3)}\sum_n\frac{|\langle\Phi_0^0|\frac{\partial V}{\partial Z}|\Phi_n^0\rangle|^2}{E_n-E_0+2Bhc(l+1)}\\&+\frac{l(l-1)+m^2}{2(2l+1)(2l-1)}\sum_n\frac{|\langle\Phi_0^0|\frac{\partial V}{\partial X}+\frac{\partial V}{\partial Y}|\Phi_n^0\rangle|^2}{E_n-E_0+2Bhcl}\\&+\frac{l^2-m^2}{(2l+1)(2l-1)}\sum_n\frac{|\langle\Phi_0^0|\frac{\partial V}{\partial Z}|\Phi_n^0\rangle|^2}{E_n-E_0+2Bhcl}\Bigg\}.\end{aligned} \tag{75}$$

For an O_h symmetry cage, these expressions are simplified and the total correction becomes:

$$\begin{aligned}\Delta E_l = d^2&\left\langle\Phi_0^0\left|\frac{\partial^2 V}{\partial X^2}\right|\Phi_0^0\right\rangle\\&-\frac{d^2}{2l+1}\left\{(l+1)\sum_n\frac{|\langle\Phi_0^0|\frac{\partial V}{\partial X}|\Phi_n^0\rangle|^2}{E_n-E_0+2Bhc(l+1)}+l\sum_n\frac{|\langle\Phi_0^0|\frac{\partial V}{\partial X}|\Phi_n^0\rangle|^2}{E_n-E_0+2Bhc(l+1)}\right\}.\end{aligned} \tag{76}$$

The correction contains a term which does not depend upon the molecular rotational state and a contribution which is a function of the rotational quantum number l. For a centrosymmetric molecule, $d = 1$ and the rotational levels remain unperturbed. Assuming $V(X, Y, Z)$ to be an harmonic potential corresponding to the frequency ω and taking $\sigma = \omega/B$, one obtains for the S_0 frequency shift:

$$\Delta\nu = -\frac{8\pi^2 Mc\omega^4 d^2}{B^2 h}\left[\frac{6}{(\sigma+6)(\sigma+2)(\sigma-4)\sigma}\right]. \tag{77}$$

$\Delta\nu = f(\omega)$ is plotted in fig. 6 for HD (B = 45,655 cm^{-1}). The frequency shifts observed in the different rare gases are reported in this figure and appear to be in satisfactory

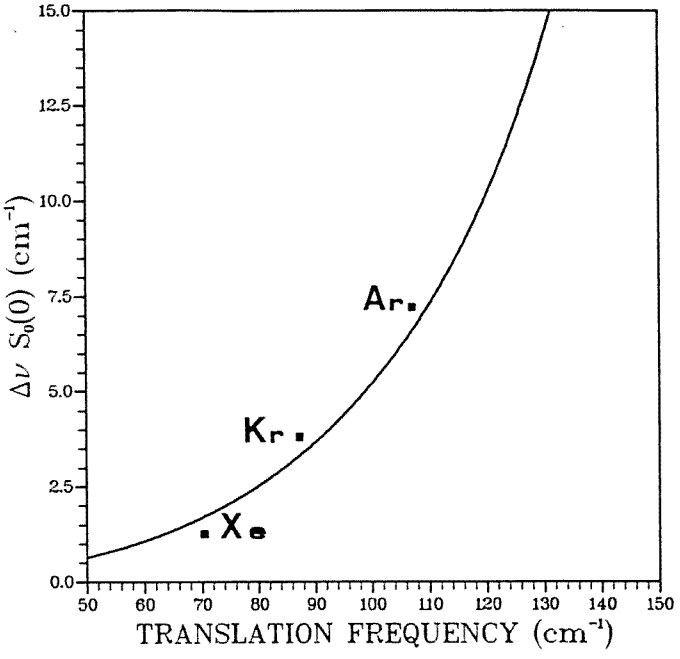

Fig. 6. S_0 frequency shift versus translation frequency.

agreement with the calculation. This model is therefore suitable to explain the anomalous shifts observed for HD.

8. Conclusion

The use of different levels of approximation in the calculation of the rovibrational frequency shifts of isotropic hydrogen molecules embedded in a rare gas matrix shows the importance of a convenient treatment of the impurity translational motion. On the one hand, unless it is not treated quantum mechanically, the calculated shifts are too large by about 50%. On the other hand, for the HD species, the rotation–translation coupling must be introduced to explain the blue shifts observed in argon and krypton for the pure rotational transition. It must be noted that the small discrepancies between the calculated results [15–18] and the previous experimental ones [7,8] suggested to Alikhani et al. to reinvestigate the spectra [11–13]. These authors were able to rationalize the experimental data, in particular, to discriminate the lines due to polymeric species from those belonging to true monomers and to evidence the anomalous blue shift of the HD $S_0(0)$ transition frequency.

References

[1] W. Whittle, D.A. Dows and G.C. Pimentel, J. Chem. Phys. 22(1954)1943.
[2] J.P. Perchard, J. Chim. Phys. 83(1986)283.

[3] R.J. Le Roy and J. Carley, *Advances in Chemical Physics*, ed. K.P. Lawley (Wiley, New York, 1980).
[4] R. Kriegler and H. Welsh, Can. J. Phys. 46(1968)1181.
[5] J. De Remigis and H. Welsh, Can. J. Phys. 48(1970)1622.
[6] G.R. Smith, J.A. Warren and W.A. Guillory, J. Chem. Phys. 65(1976)1591.
[7] G. Prochaska and L. Andrews, J. Chem. Phys. 67(1977)1139.
[8] J.A. Warren, G.R. Smith and W.A. Guillory, J. Chem. Phys. 72(1980)4901.
[9] H. Jodl and K. Bier, in: *Vibrational Spectra and Structure*, Vol. 13, ed. J.R. Durig (Elsevier, Amsterdam, 1984), p. 285.
[10] K.D. Bier, H.J. Jodl and H. Däufer, Can. J. Phys. 66(1988)708.
[11] M.E. Alikhani, B. Silvi, J.P. Perchard and V. Chandrasekharan, J. Chem. Phys. 90(1989)5221.
[12] M.E. Alikhani, L. Manceron and J.P. Perchard, J. Chem. Phys. 92(1990)22.
[13] M.E. Alikhani, L. Manceron and J.P. Perchard, Chem. Phys. 140(1990)51.
[14] J. Vitko and C.F. Coll III, Jr., J. Chem. Phys. 69(1966)135.
[15] V. Chandrasekharan, M. Chergui, B. Silvi and R.D. Etters, Physica 131B(1985)267.
[16] B. Silvi, V. Chandrasekharan, M. Chergui and R.D. Etters, Phys. Rev. B33(1986)2749.
[17] R.D. Etters, B. Silvi, V. Chandrasekharan and M. Chergui, Int. J. Quant. Chem. S19(1986)675.
[18] B. Silvi, V. Chandrasekharan, M. Chergui and R.D. Etters, J. Phys. Chem. 91(1967)1623.
[19] R.D. Etters, R. Danilowicz and W. England, Phys. Rev. A33(1975)2199.
[20] M.N. Korobov, *Teoretiko-tchislovie metodi v priblizhenom analize* (Gosudarstvennoe Izdatel'stvo, Fiziko-Matematitcheskii Literaturi, Moscow, 1963), pp. 216–222.
[21] S. Kirkpatrick, C.D. Gelatt and M.P. Vecchi, Science 220(1983)671.
[22] H. Hamaguchi, I. Suzuki and A. Buckingham, Mol. Phys. 43(1981)963.
[23] R.A. Aziz and H. Chen. J. Chem. Phys. 67(1977)5719.
[24] R.A. Aziz, Mol. Phys. 38(1979)177.
[25] J. Barker, R. Watts, J.K. Lee, T. Scharfer and Y.T. Lee, J. Chem. Phys. 46(1968)1181.
[26] H. Friedmann and S. Kimel, J. Chem. Phys. 43(1965)3925.
[27] M. Allavena and J. Rios, Cr. Acad. Sci. 263(1966)966.
[28] F.E. Harris, Rev. Mod. Phys. 35(1963)558.